J. Plasma Phys. (2026), *vol.* 92, E132 © The Author(s), 2026. Published by Cambridge University Press.
This is an Open Access article, distributed under the terms of the Creative Commons Attribution licence (https://creativecommons.org/licenses/by/4.0/), which permits unrestricted re-use, distribution and reproduction, provided the original article is properly cited. doi:10.1017/S0022377826102232

Double-adiabatic equations of state for relativistic plasmas

A. Wierzchucka[1,2], P.J. Bilbao[1,3], A.G.R. Thomas[4], D.A. Uzdensky[1] and A.A. Schekochihin[1,2]

[1]Rudolf Peierls Centre for Theoretical Physics, University of Oxford, Oxford OX1 3PU, UK
[2]Merton College, Oxford OX1 4JD, UK
[3]Lady Margaret Hall, Oxford OX2 6QA, UK
[4]Gérard Mourou Center for Ultrafast Optical Science, University of Michigan, 2200 Bonisteel Boulevard, Ann Arbor 48109, MI, USA

Corresponding author: A. Wierzchucka, agnieszka.wierzchucka@merton.ox.ac.uk

(Received 10 April 2026 UTC; revision received 23 July 2026 UTC; accepted 27 July 2026 UTC)

The adiabatic equation of state $P \propto n^{\Gamma}$ describes the pressure evolution of highly collisional, isotropic plasmas in terms of their density, providing a possible closure of the fluid moment hierarchy in the absence of heat fluxes and dissipation. An analogous closure exists for collisionless, magnetised plasmas, whose pressure tensor is anisotropic with respect to the magnetic field, and the closure is therefore double adiabatic, prescribing the evolution of the parallel and perpendicular pressures in terms of the magnetic-field strength and density. Here, we present a general first-principles formalism to derive adiabatic laws using symmetries and phase-space conservation properties of the distribution function. With this theory we recover the adiabatic equation of state $P \propto n^{\Gamma}$ for isotropic plasmas and the double-adiabatic equations of state for collisionless, magnetised plasmas. We extend the latter to the relativistic regime, finding that their exact functional form depends on the pressure anisotropy and is not a simple power law. Our double-adiabatic equations of state describe simple geometries, like magnetic mirrors or compressed homogeneous plasmas, as well as complex high-energy astrophysical processes, such as the evolution of plasmoid structures formed during magnetic reconnection.

Key words: astrophysical plasmas, plasma dynamics, plasma properties

1. Introduction

In magnetised, collisionless plasmas, constituent particles gyrate rapidly around magnetic-field lines while experiencing infrequent Coulomb collisions. Consequently, the particle gyration frequency sets the shortest time scale in the system, whereas the Coulomb collision time is the largest. Studies of collisionless and weakly collisional magnetised plasmas in the non-relativistic regime have provided significant insight into the dynamics governing space and astrophysical environments such as the solar wind (Hellinger *et al.* 2006; Bale *et al.* 2009), the Earth's magnetosphere (Øieroset *et al.* 2001; Burch *et al.* 2016), and the intracluster medium

Downloaded from https://www.cambridge.org/core. UNIVERSIDAD AUTONOMA METROPOLITANA, on 19 Nov 2026 at 08:19:22, subject to the Cambridge Core terms of use, available at https://www.cambridge.org/core/terms. https://doi.org/10.1017/S0022377826102232

(Schekochihin & Cowley 2006; Kunz, Jones & Zhuravleva 2022). Collisionless plasmas are also abundant in high-energy relativistic astrophysical systems, like pulsar-wind nebulae (Kargaltsev *et al.* 2015), pulsar magnetospheres (Cerutti & Beloborodov 2017; Philippov & Kramer 2022), accretion flows onto black holes (Rees *et al.* 1982; Narayan & Yi 1995; Quataert 2003; Yuan & Narayan 2014), and jets from active galactic nuclei (e.g. blazars) (Begelman, Blandford & Rees 1984; Blandford, Meier & Readhead 2019). Many of these sources exhibit pronounced non-thermal emission spectra, providing direct observational evidence that the associated plasmas are far from Maxwellian equilibrium. Such departure from thermal equilibrium means that studying collisionless magnetised plasmas is challenging and requires a kinetic approach.

Rapid gyromotion renders the particle distribution function azimuthally symmetric in velocity space about the magnetic field, a property known as gyrotropy. The pressure tensor in such a plasma is diagonal. When the magnetic field varies on time scales much longer than the gyration period, the first adiabatic invariant, μ, which is the angular momentum of a particle on a Larmor orbit, is conserved (Gardner 1959), leading to a non-identical evolution of the perpendicular and parallel pressures, $P_\perp$ and $P_\parallel$. In the non-relativistic limit, this evolution is described by the Chew–Goldberger–Low (CGL) equations (Chew, Goldberger & Low 1956), which express the Lagrangian evolution of $P_\perp$ and $P_\parallel$ in terms of the particle number density, n, and magnetic-field strength, B, as well as heat fluxes. When the latter can be neglected, the CGL equations are known as the double-adiabatic approximation and provide a practical fluid closure of the system: in a moving fluid element, $P_\perp$ and $P_\parallel$ are linked to the density and magnetic-field strength by instantaneous adiabatic equations of state (EoSs), $P_\perp \propto nB$ and $P_\parallel \propto n^3/B^2$. These relations are the anisotropic generalisation of the familiar adiabatic EoS $P \propto n^\Gamma$ of a highly collisional, isotropic plasma, where the adiabatic index Γ ranges from $5/3$ in the non-relativistic regime to $4/3$ in the ultra-relativistic limit (Synge 1957).

When heat fluxes can be neglected, the CGL equations are sometimes referred to as 'double adiabatic' because they encompass the conservation of two adiabatic invariants, the first being the aforementioned μ. The second adiabatic invariant, J, is associated with the trapping and bouncing of particles in magnetic mirrors and remains conserved under the condition that this bouncing is much faster than the fluid motions. Such a requirement is much more restrictive than that of rapid gyration, and so the conservation of J is less robust than the conservation of μ. The conservation of these two quantities can be shown through the use of action-angle variables (Gardner 1959; Kruskal 1962) or directly by expanding the particle equations of motion in small gyration periods, an approximation known as drift kinetics (Northrop & Teller 1960; Vandervoort 1960; Northrop 1963).

The double-adiabatic equations give insight into the various processes governing the dynamics of collisionless plasmas. As they predict different evolution of $P_\perp$ and $P_\parallel$, local changes in the density or magnetic field, e.g. due to shearing or compressing flows, can give rise to local pressure anisotropies (Hellinger & Trávníček 2008; Kunz, Schekochihin & Stone 2014; Sironi & Narayan 2015). In high-β plasmas, where β is the ratio of the thermal to magnetic pressure, pressure anisotropy can lead to the excitation of various kinetic instabilities (see Bott, Cowley & Schekochihin 2024 and references therein). When the anisotropy, $\Delta \equiv P_\perp/P_\parallel - 1$, is positive, the mirror (Hasegawa 1969; Southwood & Kivelson 1993) and ion-cyclotron instabilities emerge if $\Delta \gtrsim 1/\beta$. In the opposite case, if $\Delta \lesssim -2/\beta$, the microscale dynamics of the plasma becomes dominated by the firehose instability

Downloaded from https://www.cambridge.org/core. UNIVERSIDAD AUTONOMA METROPOLITANA, on 19 Nov 2026 at 08:19:22, subject to the Cambridge Core terms of use, available at https://www.cambridge.org/core/terms. https://doi.org/10.1017/S0022377826102232

(Chandrasekhar, Kaufman & Watson 1958). After a short period of exponential growth, both the mirror and firehose instabilities saturate and, albeit through different mechanisms, pin the pressure anisotropy to their respective thresholds (Melville, Schekochihin & Kunz 2016; Bott *et al.* 2025). As a result, the pressure becomes nearly isotropic and evolves with an adiabatic index $\Gamma = 5/3$ in the high-β non-relativistic regime.

As the distribution function is gyrotropic to lowest order in the gyration period, the Vlasov equation can be averaged over the gyromotion to obtain the so-called drift-kinetic equation. This constitutes a starting point for studying the kinetic instabilities excited in collisionless plasmas, although finite-gyroradius effects must be included to recover the fastest-growing modes (Yoon, Wu & de Assis 1993; Hellinger 2007; Bott *et al.* 2024).

The CGL equations are derived by taking perpendicular and parallel pressure moments of the drift-kinetic equation (see e.g. Schekochihin *et al.* 2010 for a derivation). This procedure can be extended to relativistic collisionless plasmas (Gedalin & Oiberman 1995; Hegade & Stone 2026; Wierzchucka *et al.* 2026*b*). Unlike in the non-relativistic regime, the relativistic CGL equations do not provide an evolution equation for the two pressures. Instead, they evolve related quantities that we refer to below as the modified pressures. However, as it is the pressures, and not the modified pressures, that are needed in the fluid momentum equation, this means that, relativistically, the generalised CGL equations cannot provide a sufficient fluid closure of the system. Describing the evolution of $P_\perp$ and $P_\parallel$ in a relativistic, collisionless, magnetised plasma is somewhat non-trivial. The main reason for this is that, in the relativistic case, the momentum-space integration in the definition of $P_\perp$ and $P_\parallel$ involves, in addition to the corresponding momentum components, the particle Lorentz factor γ, which is a nonlinear function of the perpendicular and parallel momenta. As a result, $P_\perp$ ($P_\parallel$) depends not only on the perpendicular (parallel) component of the particle momentum but also on the total momentum (through the Lorentz factor). In other words, each pressure component depends on the full momentum distribution rather than solely on its corresponding momentum projection, as in the non-relativistic case. Therefore, their evolution in the double-adiabatic limit, i.e. in the absence of heat fluxes, turns out to depend not only on the density and magnetic-field strength but also on the pressure anisotropy.

In this paper, we derive the double-adiabatic equations satisfied by $P_\perp$ and $P_\parallel$ in relativistic collisionless plasmas, with a non-relativistic bulk flow. We do this by abandoning the standard moment-based derivation of the evolution equations and instead formulating a theory of adiabatic invariance focused on the system's symmetries. Through the use of phase-space volume conservation properties, we show that imposing certain symmetries leads to a self-similar evolution of the distribution function. Calculating the pressure moments of the evolved distribution then yields the adiabatic EoSs, whose form, in general, depends on the distribution at some initial (reference) time. For example, one can easily show that a distribution function isotropic in peculiar momentum satisfies $P \propto n^{5/3}$ and $P \propto n^{4/3}$ in the non-relativistic and ultra-relativistic regimes, respectively. If the distribution function is gyrotropic and has parity symmetry along the magnetic-field direction in the peculiar-momentum coordinate, we find by the same procedure that the double-adiabatic equations, $P_\perp \propto nB$ and $P_\parallel \propto n^3/B^2$, hold in the non-relativistic limit.

Using this symmetry-based approach, we extend the double-adiabatic equations to the relativistic regime. We study these equations for the case of an ultra-relativistically hot plasma with an isotropic reference distribution. We find that the

Downloaded from https://www.cambridge.org/core. UNIVERSIDAD AUTONOMA METROPOLITANA, on 19 Nov 2026 at 08:19:22, subject to the Cambridge Core terms of use, available at https://www.cambridge.org/core/terms. https://doi.org/10.1017/S0022377826102232

exact form of the double-adiabatic equations depends on the pressure anisotropy and derive the asymptotic theory for three main limiting cases. When $P_\perp \gg P_\parallel$ ($\Delta \gg 1$), we find $P_\perp \propto nB^{1/2}$ and $P_\parallel \propto n^3/B^{5/2}$, whereas when $P_\parallel \gg P_\perp$ ($\Delta \approx -1$), we find $P_\perp \propto B^2 \ln(n'^2/B'^3)$ and $P_\parallel \propto n^2/B$. Here, B' and n' are, respectively, the relative changes in the magnetic-field strength and density. These evolution equations agree with the initial discussion of the relativistic CGL equations in Gedalin & Oiberman (1995), up to the logarithmic correction in the second $P_\perp$ expression. In contrast, close to isotropy, i.e. when $|\Delta| \ll 1$, we find $P_\perp \propto (nB)^{4/5}$ and $P_\parallel \propto (n^3/B^2)^{4/5}$. Our results differ drastically from the non-relativistic theory (Chew *et al.* 1956), in which the same double-adiabatic relations hold for all anisotropies. We confirm our predictions using two-dimensional particle-in-cell (PIC) simulations incorporating a large-scale compressive flow.

In situations where heat fluxes are negligible, these double-adiabatic equations can be the EoSs for relativistic collisionless plasmas. Such EoSs are crucial for modelling large-scale high-energy astrophysical systems by means of a fluid theory, e.g. to determine regions where kinetic processes like the firehose and mirror instabilities are excited in high-β plasmas. Their applicability to the relativistic regime also means that our EoSs can be coupled to other high-energy processes, such as synchrotron cooling, providing a pathway to modelling phenomena like the recently discovered synchrotron firehose instability (Zhdankin, Kunz & Uzdensky 2023). Double-adiabatic EoSs may additionally have an important effect on the large-scale magnetohydrodynamic-equilibrium structure of astrophysical magnetospheres and flows (Beskin & Kuznetsova 2000).

2. Adiabatic invariance and symmetries

We consider a particle distribution function $f(\boldsymbol{r}, \boldsymbol{p}, t)$, where $\boldsymbol{r}$ and $\boldsymbol{p}$ denote the position and momentum variables, and t denotes time. The distribution function is the density of a phase-space fluid filling the six-dimensional $(\boldsymbol{r}, \boldsymbol{p})$ space, moving with velocity

$$\dot{\boldsymbol{r}} = \boldsymbol{v}, \quad \dot{\boldsymbol{p}} = \boldsymbol{F}. \tag{2.1}$$

The velocity coordinate $\boldsymbol{v}$ is related to the momentum through $\boldsymbol{p} = \gamma m \boldsymbol{v}$, where $\gamma = \sqrt{1 + (p/mc)^2}$ is the Lorentz factor, and m is the particle mass. The force $\boldsymbol{F}$ depends on the particular physical system that the distribution function describes. In this paper, we focus on Hamiltonian systems, in which case the phase-space fluid has the additional property of being incompressible.

To describe how f evolves in time, we adopt a Lagrangian formalism (Newcomb 1961). We describe the position of an infinitesimal fluid element in phase space using not its current coordinates $(\boldsymbol{r}, \boldsymbol{p})$, but instead its position at $t = 0$, $(\boldsymbol{r}_0, \boldsymbol{p}_0)$. In this approach, the conservation of probability is

$$\mathrm{d}\boldsymbol{r}\mathrm{d}\boldsymbol{p}\ f(t, \boldsymbol{r}, \boldsymbol{p}) = \mathrm{d}\boldsymbol{r}_0\mathrm{d}\boldsymbol{p}_0\ f_0(\boldsymbol{r}_0, \boldsymbol{p}_0), \tag{2.2}$$

and the incompressibility of the phase-space fluid, also referred to as the conservation of phase-space volume, is written as

$$\left| \frac{\partial(\boldsymbol{r}, \boldsymbol{p})}{\partial(\boldsymbol{r}_0, \boldsymbol{p}_0)} \right| = 1. \tag{2.3}$$

One can combine (2.2) and (2.3) to find Liouville's theorem

$$f(t, \boldsymbol{r}, \boldsymbol{p}) = f_0(\boldsymbol{r}_0, \boldsymbol{p}_0), \tag{2.4}$$

where f_0 is the distribution function at $t = 0$.

Downloaded from https://www.cambridge.org/core. UNIVERSIDAD AUTONOMA METROPOLITANA, on 19 Nov 2026 at 08:19:22, subject to the Cambridge Core terms of use, available at https://www.cambridge.org/core/terms. https://doi.org/10.1017/S0022377826102232

Two important moments of f are the density and the Eckart (1940) bulk velocity, defined, respectively, by

$$n \equiv \int \mathrm{d}\boldsymbol{p}\ f, \quad n\boldsymbol{u} \equiv \int \mathrm{d}\boldsymbol{p}\ \boldsymbol{v} f. \tag{2.5}$$

In this work, for simplicity, we restrict our analysis to the non-relativistic limit as far as the bulk velocity of the plasma is concerned, $|\boldsymbol{u}| \ll c$. Nevertheless, our findings regarding the adiabatic and double-adiabatic EoSs remain valid in the fully relativistic regime, as discussed in § 5. We label quantities in the comoving frame with a tilde, referring to them as 'peculiar'. To first order in $|\boldsymbol{u}|/c$, the Lorentz transformation of the momentum to the peculiar momentum is

$$\boldsymbol{p} = \tilde{\gamma} m \boldsymbol{u} + \tilde{\boldsymbol{p}}, \tag{2.6}$$

and the corresponding transformation of the Lorentz factor is

$$\gamma = \frac{\boldsymbol{u} \cdot \tilde{\boldsymbol{p}}}{mc^2} + \tilde{\gamma}. \tag{2.7}$$

The Jacobian of this change of variables is, again to first order in $|\boldsymbol{u}|/c$,

$$\left| \frac{\partial \boldsymbol{p}}{\partial \tilde{\boldsymbol{p}}} \right| = 1 + \frac{\boldsymbol{u} \cdot \tilde{\boldsymbol{v}}}{c^2}, \tag{2.8}$$

where $\tilde{\boldsymbol{v}} = \tilde{\boldsymbol{p}}/\tilde{\gamma} m$. In the fully non-relativistic regime, $|\tilde{\boldsymbol{p}}| \ll mc$, (2.6) reduces to $\boldsymbol{p} = m\boldsymbol{u} + \tilde{\boldsymbol{p}}$, as expected. Note that, while by definition of the bulk velocity (2.5), $\int \mathrm{d}\tilde{\boldsymbol{p}}\ \tilde{\boldsymbol{v}} f = 0$, in general $\int \mathrm{d}\tilde{\boldsymbol{p}}\ \tilde{\boldsymbol{p}} f \neq 0$, reflecting the differences between the Landau (Landau & Lifshitz 1987) and Eckart bulk velocities.

2.1. *Isotropy*

For illustration, we first consider a distribution function that evolves in such a way as to remain isotropic in the frame moving with $\boldsymbol{u}$. This could arise, e.g. due to efficient pitch-angle scattering dominating the system's dynamics, and implies the neglect of heat fluxes. Introducing spherical polar coordinates $(\tilde{p}, \theta, \phi)$, with the polar axis orientated in an arbitrary direction, we have

$$\tilde{\boldsymbol{p}} = \tilde{p}(\cos\phi \sin\theta \hat{\boldsymbol{x}} + \sin\phi \sin\theta \hat{\boldsymbol{y}} + \cos\theta \hat{\boldsymbol{z}}), \tag{2.9}$$

and the corresponding Jacobian is

$$\left| \frac{\partial \tilde{\boldsymbol{p}}}{\partial(\tilde{p}, \theta, \phi)} \right| = \tilde{p}^2 \sin\theta. \tag{2.10}$$

The isotropy assumption is then the statement that

$$f = f(t, \boldsymbol{r}, \tilde{p}). \tag{2.11}$$

We assume that in this 'reduced phase space', phase-space volume is conserved, i.e.

$$\left| \frac{\partial(\boldsymbol{r}, \tilde{p})}{\partial(\boldsymbol{r}_0, \tilde{p}_0)} \right| = \frac{\tilde{p}_0^2}{\tilde{p}^2}, \tag{2.12}$$

Downloaded from https://www.cambridge.org/core. UNIVERSIDAD AUTONOMA METROPOLITANA, on 19 Nov 2026 at 08:19:22, subject to the Cambridge Core terms of use, available at https://www.cambridge.org/core/terms. https://doi.org/10.1017/S0022377826102232

where we have made use of (2.10). Combining (2.12) with Liouville's theorem (2.4) then implies the conservation of probability

$$\mathrm{d}\boldsymbol{r}\,\mathrm{d}\tilde{p}\;\tilde{p}^2 f(t,\boldsymbol{r},\tilde{p}) = \mathrm{d}\boldsymbol{r}_0\mathrm{d}\tilde{p}_0\;\tilde{p}_0^2 f_0(\boldsymbol{r}_0,\tilde{p}_0). \tag{2.13}$$

Considering a rapidly isotropised distribution function is equivalent to assuming that the phase space can be described by its average over some fast time scale t_{fast} associated with the isotropisation process. In the laboratory frame, such an average is defined by

$$\langle\cdot\rangle_{t_{\mathrm{fast}}} \equiv \frac{\int_t^{t+t_{\mathrm{fast}}}(\cdot)\,\mathrm{d}t}{\int_t^{t+t_{\mathrm{fast}}}\mathrm{d}t}. \tag{2.14}$$

However, isotropisation is a microscopic process that occurs in the particle's proper time τ, which is related to the laboratory time via $\mathrm{d}t = \gamma\,\mathrm{d}\tau$. We assume that, during this process, the particle's motion becomes uniformly randomised as far as its direction is concerned, allowing the proper-time average to be replaced by an average over the solid angle of the peculiar momentum. Therefore,

$$\langle\cdot\rangle_{t_{\mathrm{fast}}} = \frac{\int_\tau^{\tau+\tau_{\mathrm{fast}}}(\cdot)\gamma\,\mathrm{d}\tau}{\int_\tau^{\tau+\tau_{\mathrm{fast}}}\gamma\,\mathrm{d}\tau} = \frac{\iint(\cdot)\gamma\;\sin\theta\,\mathrm{d}\theta\mathrm{d}\phi}{\iint\gamma\;\sin\theta\,\mathrm{d}\theta\mathrm{d}\phi} = \frac{\langle\gamma(\cdot)\rangle_{\theta,\phi}}{\langle\gamma\rangle_{\theta,\phi}}. \tag{2.15}$$

Thus, in the relativistic limit, replacing the averaging over fast time scales with angle averaging leads to the appearance of a Lorentz factor inside the angle integrals. As expected, in the non-relativistic limit, where $\gamma \approx 1$, these averages are the same.

Averaging the phase-space flow (2.1) via (2.15) gives $\langle\dot{\boldsymbol{r}}\rangle_{t_{\mathrm{fast}}} = \boldsymbol{u}$, where we have used (2.6) and (2.7). Consequently, in the reduced phase space, the mapping between $\boldsymbol{r}$ and $\boldsymbol{r}_0$ is independent of the peculiar coordinates. The phase-space path $\boldsymbol{r} = \boldsymbol{r}(t,\boldsymbol{r}_0)$ then corresponds to that of a fluid element advected with the bulk velocity $\boldsymbol{u}$ in three-dimensional position space. The Jacobian (2.12) therefore factorises into spatial and momentum parts

$$\left|\frac{\partial(\boldsymbol{r},\tilde{p})}{\partial(\boldsymbol{r}_0,\tilde{p}_0)}\right| = \left|\frac{\partial\boldsymbol{r}}{\partial\boldsymbol{r}_0}\right|\frac{\partial\tilde{p}}{\partial\tilde{p}_0}. \tag{2.16}$$

We can calculate the first factor in (2.16) by returning to (2.13), integrating over the momenta, and recalling the definition of density (2.5) to find

$$\mathrm{d}\boldsymbol{r}\;n(t,\boldsymbol{r}) = \mathrm{d}\boldsymbol{r}_0\;n_0(\boldsymbol{r}_0), \tag{2.17}$$

which implies

$$\left|\frac{\partial\boldsymbol{r}_0}{\partial\boldsymbol{r}}\right| = \frac{n(t,\boldsymbol{r})}{n_0(\boldsymbol{r}_0)} \equiv n'(t,\boldsymbol{r}_0). \tag{2.18}$$

Combining the above expression with (2.16) and inserting the result into (2.12) yields a differential equation whose solution is

$$\tilde{p}_0 = \frac{\tilde{p}}{n'^{1/3}}. \tag{2.19}$$

Downloaded from https://www.cambridge.org/core. UNIVERSIDAD AUTONOMA METROPOLITANA, on 19 Nov 2026 at 08:19:22, subject to the Cambridge Core terms of use, available at https://www.cambridge.org/core/terms. https://doi.org/10.1017/S0022377826102232

We can now substitute (2.19) into Liouville's theorem (2.4) and find the evolution of the distribution function

$$f(t, \boldsymbol{r}, \tilde{p}) = f_0\left(\boldsymbol{r}_0, \frac{\tilde{p}}{n'^{1/3}}\right). \tag{2.20}$$

Note that the explicit form of $\boldsymbol{r}(t, \boldsymbol{r}_0)$ is not required, as the trajectory corresponds to that of a fluid element advected with the bulk velocity $\boldsymbol{u}$. Hence, any evolution equations obtained by taking moments of (2.20) are Lagrangian relations with respect to $\boldsymbol{u}$.

2.1.1. Equation of state for isotropic plasma

Now that we have found how the distribution function evolves, we can work out the corresponding EoS. In the relativistic regime, pressure is given by

$$P = \frac{1}{3m}\int \mathrm{d}\tilde{\boldsymbol{p}}\,\frac{\tilde{p}^2}{\tilde{\gamma}}\,f. \tag{2.21}$$

Inserting (2.20) into (2.21), integrating over θ and ϕ, and changing the momentum integration variable to $\tilde{p}_0$ via (2.19) gives the adiabatic EoS for an isotropic plasma

$$P = \frac{4\pi n'^{5/3}}{3m}\int \mathrm{d}\tilde{p}_0\,\frac{\tilde{p}_0^4 f_0(\tilde{p}_0)}{\sqrt{1 + n'^{2/3}\,(\tilde{p}_0/mc)^2}}. \tag{2.22}$$

In the non-relativistic regime, $\tilde{p} \ll mc$, (2.22) reduces to the familiar scaling $P \propto n^{5/3}$ and in the ultra-relativistic limit, $\tilde{p} \gg mc$, we instead obtain $P \propto n^{4/3}$, as expected. In general, however, P depends not solely on density but also on the form of the initial distribution function $f_0(\tilde{p})$. Substituting the Maxwell–Jüttner distribution into (2.22) recovers the Synge gas EoS (Synge 1957).

2.2. *Gyrotropy and parity*

We now consider a more general case, where the isotropy assumption is relaxed but the distribution function still satisfies two symmetries in the peculiar-momentum coordinate. First, it is gyrotropic, i.e. it has cylindrical symmetry with respect to some vector field, which we call $\boldsymbol{B}$. Second, the distribution function has parity symmetry along this vector. We assume that the vector $\boldsymbol{B}$ is divergence free and frozen into the bulk flow; it therefore satisfies the induction equation

$$\frac{\partial \boldsymbol{B}}{\partial t} = \boldsymbol{\nabla} \times (\boldsymbol{u} \times \boldsymbol{B}). \tag{2.23}$$

For example, in a drift-kinetic plasma, $\boldsymbol{B}$ corresponds to the magnetic field (Kulsrud 1964). A distribution function with such symmetries can arise in systems where fast processes, such as gyromotion or the bouncing of trapped particles in magnetic mirrors of collisionless plasmas, dominate the dynamics, and implies the neglect of heat fluxes.[1]

[1] Double-adiabatic EoSs hold if certain combinations of parallel-heat-flux terms vanish at all times. The parity condition is a sufficient condition for this to happen; it is not currently known whether it is also necessary.

Downloaded from https://www.cambridge.org/core. UNIVERSIDAD AUTONOMA METROPOLITANA, on 19 Nov 2026 at 08:19:22, subject to the Cambridge Core terms of use, available at https://www.cambridge.org/core/terms. https://doi.org/10.1017/S0022377826102232

We adopt a cylindrical coordinate system in the peculiar-momentum space $(\tilde{p}_\perp, \phi, \tilde{p}_\parallel, \sigma)$, with the polar axis parallel to $\boldsymbol{b} \equiv \boldsymbol{B}/B$

$$\tilde{\boldsymbol{p}} = \tilde{p}_\perp(\cos\phi\hat{\boldsymbol{x}} + \sin\phi\hat{\boldsymbol{y}}) + \sigma\,\tilde{p}_\parallel \boldsymbol{b}, \tag{2.24}$$

where $\tilde{p}_\parallel \geqslant 0$ and σ takes the values $+1$ or -1, labelling the direction of the parallel peculiar momentum. The Jacobian of this change of variables is

$$\left|\frac{\partial\tilde{\boldsymbol{p}}}{\partial(\tilde{p}_\perp, \phi, \tilde{p}_\parallel)}\right| = \tilde{p}_\perp. \tag{2.25}$$

The gyrotropy and parity assumptions are then equivalent to imposing that f is independent of ϕ and σ

$$f = f(t, \boldsymbol{r}, \tilde{p}_\perp, \tilde{p}_\parallel). \tag{2.26}$$

We again assume that phase-space volume in the reduced phase space is conserved, *viz*.

$$\left|\frac{\partial(\boldsymbol{r}, \tilde{p}_\perp, \tilde{p}_\parallel)}{\partial(\boldsymbol{r}_0, \tilde{p}_{\perp 0}, \tilde{p}_{\parallel 0})}\right| = \frac{\tilde{p}_{\perp 0}}{\tilde{p}_\perp}, \tag{2.27}$$

where we have made use of (2.25). Combining Liouville's theorem (2.4) with (2.27) yields the conservation of probability (2.2) in our reduced phase space

$$\mathrm{d}\boldsymbol{r}\mathrm{d}\tilde{p}_\perp\mathrm{d}\tilde{p}_\parallel\ \tilde{p}_\perp f(t, \boldsymbol{r}, \tilde{p}_\perp, \tilde{p}_\parallel) = \mathrm{d}\boldsymbol{r}_0\mathrm{d}\tilde{p}_{\perp 0}\mathrm{d}\tilde{p}_{\parallel 0}\ \tilde{p}_{\perp 0} f_0(\boldsymbol{r}_0, \tilde{p}_{\perp 0}, \tilde{p}_{\parallel 0}). \tag{2.28}$$

In analogy to § 2.1, imposing (2.26) is equivalent to assuming that the phase space is well described by its average over some fast time scales associated with the two symmetries (e.g. Larmor gyration and bouncing inside magnetic mirrors). In the non-relativistic limit, averaging over these time scales in the laboratory frame is equivalent to an average over σ and ϕ. In the relativistic case, as in (2.15), the average acquires a weight of γ

$$\langle\cdot\rangle_{t_{\mathrm{fast}}} \equiv \frac{\int_t^{t+t_{\mathrm{fast}}}(\cdot)\mathrm{d}t}{\int_t^{t+t_{\mathrm{fast}}}\mathrm{d}t} = \frac{\sum_\sigma\int(\cdot)\gamma\,\mathrm{d}\phi}{\sum_\sigma\int\gamma\,\mathrm{d}\phi} = \frac{\langle\gamma(\cdot)\rangle_{\phi,\sigma}}{\langle\gamma\rangle_{\phi,\sigma}}. \tag{2.29}$$

Averaging the phase-space flow (2.1) over the fast time scales using (2.6), (2.7), and (2.29) gives $\langle\dot{\boldsymbol{r}}\rangle_{t_{\mathrm{fast}}} = \boldsymbol{u}$, as in § 2.1, implying that, in the reduced phase space, the trajectory $\boldsymbol{r} = \boldsymbol{r}(t, \boldsymbol{r}_0)$ again corresponds to that of a fluid element advected with the bulk flow $\boldsymbol{u}$. Hence, the Jacobian in (2.27) factorises into spatial and momentum contributions

$$\left|\frac{\partial(\boldsymbol{r}, \tilde{p}_\perp, \tilde{p}_\parallel)}{\partial(\boldsymbol{r}_0, \tilde{p}_{\perp 0}, \tilde{p}_{\parallel 0})}\right| = \left|\frac{\partial\boldsymbol{r}}{\partial\boldsymbol{r}_0}\right|\left|\frac{\partial(\tilde{p}_\perp, \tilde{p}_\parallel)}{\partial(\tilde{p}_{\perp 0}, \tilde{p}_{\parallel 0})}\right|, \tag{2.30}$$

where the former can be evaluated using (2.18). Then, from (2.30) and (2.27), we have

$$\left|\frac{\partial(\tilde{p}_\perp, \tilde{p}_\parallel)}{\partial(\tilde{p}_{\perp 0}, \tilde{p}_{\parallel 0})}\right| = \frac{\tilde{p}_{\perp 0}}{\tilde{p}_\perp} n'(t, \boldsymbol{r}_0). \tag{2.31}$$

Downloaded from https://www.cambridge.org/core. UNIVERSIDAD AUTONOMA METROPOLITANA, on 19 Nov 2026 at 08:19:22, subject to the Cambridge Core terms of use, available at https://www.cambridge.org/core/terms. https://doi.org/10.1017/S0022377826102232

To determine the evolution of f, we require expressions for $\tilde{p}_\perp$ and $\tilde{p}_\parallel$ in terms of their initial values. However, we have obtained only a single constraint (2.31). We therefore assume that, in addition to phase-space volume, the phase-space area perpendicular to $\boldsymbol{B}$ is conserved. A natural coordinate system for resolving directions parallel and perpendicular to $\boldsymbol{B}$ is provided by the Clebsch variables (α, β, ℓ), defined by

$$\boldsymbol{B} = \nabla\alpha \times \nabla\beta, \quad \nabla\ell = \boldsymbol{b}. \tag{2.32}$$

Here, α and β label a magnetic-field line, while ℓ measures distance along it. The Jacobian of this transformation is

$$\left|\frac{\partial \boldsymbol{r}}{\partial(\alpha, \beta, \ell)}\right| = \frac{1}{B(t, \boldsymbol{r})}, \tag{2.33}$$

and the conservation of perpendicular phase-space area can be written as

$$\mathrm{d}\alpha\mathrm{d}\beta\mathrm{d}\tilde{p}_\perp \; B^{-1}(t, \boldsymbol{r})\tilde{p}_\perp = \mathrm{d}\alpha_0\mathrm{d}\beta_0\mathrm{d}\tilde{p}_{\perp 0} \; B_0^{-1}(\boldsymbol{r}_0)\tilde{p}_{\perp 0} \tag{2.34}$$

or, equivalently,

$$\left|\frac{\partial(\alpha, \beta, \tilde{p}_\perp)}{\partial(\alpha_0, \beta_0, \tilde{p}_{\perp 0})}\right| = \frac{\tilde{p}_{\perp 0}}{\tilde{p}_\perp}\frac{B(t, \boldsymbol{r})}{B_0(\boldsymbol{r}_0)} \equiv \frac{\tilde{p}_{\perp 0}}{\tilde{p}_\perp}B'(t, \boldsymbol{r}_0). \tag{2.35}$$

As we discuss in § 2.2.3, this is just the conservation of μ in collisionless, magnetised plasmas, or rather the conservation of μ is how the conservation of perpendicular phase-space area is physically achieved by a plasma.

From the induction equation (2.23), we have $\dot{\alpha} = \dot{\beta} = 0$, so $\alpha = \alpha_0$ and $\beta = \beta_0$, i.e. α and β remain constant as the field is advected by the flow $\boldsymbol{u}$. Hence, (2.35) yields

$$\frac{\partial \tilde{p}_\perp}{\partial \tilde{p}_{\perp 0}} = \frac{\tilde{p}_{\perp 0}}{\tilde{p}_\perp}B'. \tag{2.36}$$

Integration of (2.36) yields

$$\tilde{p}_{\perp 0} = \frac{\tilde{p}_\perp}{\sqrt{B'}}, \tag{2.37}$$

and substituting this into (2.31) gives

$$\tilde{p}_{\parallel 0} = \frac{\tilde{p}_\parallel B'}{n'}. \tag{2.38}$$

Finally, we can combine (2.37) and (2.38) with Liouville's theorem (2.4) to find the evolved distribution function

$$f(t, \boldsymbol{r}, \tilde{p}_\perp, \tilde{p}_\parallel) = f_0\left(\boldsymbol{r}_0, \frac{\tilde{p}_\perp}{\sqrt{B'}}, \frac{\tilde{p}_\parallel B'}{n'}\right). \tag{2.39}$$

Again, the time dependence is encoded via $n'(t, \boldsymbol{r}_0)$, $B'(t, \boldsymbol{r}_0)$, and $\boldsymbol{r}(t, \boldsymbol{r}_0)$.

Downloaded from https://www.cambridge.org/core. UNIVERSIDAD AUTONOMA METROPOLITANA, on 19 Nov 2026 at 08:19:22, subject to the Cambridge Core terms of use, available at https://www.cambridge.org/core/terms. https://doi.org/10.1017/S0022377826102232

2.2.1. Equations of state for gyrotropic plasma

Similarly to § 2.1.1, we can now use the evolved distribution (2.39) to calculate the corresponding EoSs. For a relativistic plasma, the parallel and perpendicular pressures are defined by

$$P_\perp = \frac{1}{2m}\int \mathrm{d}\tilde{\boldsymbol{p}}\ \frac{\tilde{p}_\perp^2}{\tilde{\gamma}} f, \quad P_\parallel = \frac{1}{m}\int \mathrm{d}\tilde{\boldsymbol{p}}\ \frac{\tilde{p}_\parallel^2}{\tilde{\gamma}} f. \tag{2.40}$$

Inserting (2.39) into these equations, integrating over σ and ϕ, and finally changing the integration variables to $\tilde{p}_{\perp 0}$ and $\tilde{p}_{\parallel 0}$ via (2.37) and (2.38) yields the double-adiabatic pressure-evolution equations

$$P_\perp = \frac{2\pi n' B'}{m}\int \mathrm{d}\tilde{p}_{\perp 0}\ \mathrm{d}\tilde{p}_{\parallel 0} \frac{\tilde{p}_{\perp 0}^3 f_0(\tilde{p}_{\perp 0}, \tilde{p}_{\parallel 0})}{\sqrt{1 + B'\,(\tilde{p}_{\perp 0}/mc)^2 + (n'/B')^2\,(\tilde{p}_{\parallel 0}/mc)^2}}, \tag{2.41}$$

$$P_\parallel = \frac{4\pi n'^3}{mB'^2}\int \mathrm{d}\tilde{p}_{\perp 0}\ \mathrm{d}\tilde{p}_{\parallel 0} \frac{\tilde{p}_{\perp 0}\tilde{p}_{\parallel 0}^2 f_0(\tilde{p}_{\perp 0}, \tilde{p}_{\parallel 0})}{\sqrt{1 + B'\,(\tilde{p}_{\perp 0}/mc)^2 + (n'/B')^2\,(\tilde{p}_{\parallel 0}/mc)^2}}. \tag{2.42}$$

These integrals do not, in general, exhibit a single set of simple scalings with n' and B' for arbitrary f_0. However, in the non-relativistic limit, $\tilde{p}_\perp, \tilde{p}_\parallel \ll mc$, (2.41) and (2.42) reduce to the CGL equations, i.e. $P_\perp \propto nB$ and $P_\parallel \propto n^3/B^2$ (Chew *et al.* 1956), for all f_0.

2.2.2. Modified pressures

The complicated dependence of (2.41) and (2.42) on n' and B' arises due to the presence of the Lorentz factor in the integrand of (2.40). To avoid this issue, one can define the modified pressures

$$\hat{P}_\perp \equiv \frac{1}{2m}\int \mathrm{d}\tilde{\boldsymbol{p}}\ \tilde{p}_\perp^2 f, \quad \hat{P}_\parallel \equiv \frac{1}{m}\int \mathrm{d}\tilde{\boldsymbol{p}}\ \tilde{p}_\parallel^2 f. \tag{2.43}$$

Proceeding as before and inserting (2.39) into the definitions above, we find

$$\hat{P}_\perp = \frac{2\pi n' B'}{m}\int \mathrm{d}\tilde{p}_{\perp 0}\ \mathrm{d}\tilde{p}_{\parallel 0}\tilde{p}_{\perp 0}^3 f_0(\tilde{p}_{\perp 0}, \tilde{p}_{\parallel 0}), \tag{2.44}$$

$$\hat{P}_\parallel = \frac{4\pi n'^3}{mB'^2}\int \mathrm{d}\tilde{p}_{\perp 0}\ \mathrm{d}\tilde{p}_{\parallel 0}\ \tilde{p}_{\perp 0}\tilde{p}_{\parallel 0}^2 f_0(\tilde{p}_{\perp 0}, \tilde{p}_{\parallel 0}). \tag{2.45}$$

The integrals in both (2.44) and (2.45) can be replaced by the initial values of the modified pressures, $\hat{P}_{\perp 0}$ and $\hat{P}_{\parallel 0}$. We thus obtain the simple relationships

$$\hat{P}'_\perp = n' B', \quad \hat{P}'_\parallel = \frac{n'^3}{B'^2}, \tag{2.46}$$

Downloaded from https://www.cambridge.org/core. UNIVERSIDAD AUTONOMA METROPOLITANA, on 19 Nov 2026 at 08:19:22, subject to the Cambridge Core terms of use, available at https://www.cambridge.org/core/terms. https://doi.org/10.1017/S0022377826102232

where $\hat{P}'_\perp \equiv \hat{P}_\perp/\hat{P}_{\perp 0}$ and $\hat{P}'_\parallel \equiv \hat{P}_\parallel/\hat{P}_{\parallel 0}$. These expressions are the relativistic generalisation of the CGL equations. They can alternatively be derived by taking moments of the relativistic Vlasov equation and neglecting heat fluxes, as was first done in Gedalin & Oiberman (1995). However, in the fluid momentum equation, it is $P_\perp$ and $P_\parallel$ that appear, not $\hat{P}_\perp$ and $\hat{P}_\parallel$. Hence, in general, (2.46) does not provide a suitable fluid closure for collisionless relativistic plasmas.

2.2.3. Application to collisionless, magnetised plasmas

The theory presented above derives double-adiabatic evolution equations for a fluid system with a divergence-free vector field $\boldsymbol{B}$ frozen into the bulk flow. The derivation relies on a set of assumptions regarding the symmetries of the distribution function in peculiar-momentum space, as well as the conservation properties of the evolving phase-space density. First, we considered a gyrotropic distribution function and assumed conservation of phase-space area perpendicular to $\boldsymbol{B}$. Second, we imposed parity symmetry along the direction of $\boldsymbol{B}$ in peculiar-momentum space, together with conservation of the full phase-space volume.

An example of a system in which such symmetries arise as a result of fast processes is a collisionless magnetised plasma. The fast particle gyration provides the largest frequency in such a system, implying the gyrotropy of the distribution function and the conservation of the first adiabatic invariant (Gardner 1959)

$$\mu = \frac{\tilde{p}_\perp^2}{2B} \tag{2.47}$$

along gyro-averaged particle trajectories. This conservation implies (2.37) and provides the physical mechanism whereby the conservation of perpendicular phase-space area (2.34) holds. We are currently not aware of a system where such conservation is achieved by different means.

The conservation of μ can cause particles with sufficiently large pitch angles to become trapped in local minima of the magnetic-field strength (magnetic mirrors) and undergo bounce motion. If such bouncing occurs on time scales much shorter than those of the fluid motion, a second adiabatic invariant,

$$J = \oint \tilde{p}_\parallel \, \mathrm{d}\ell, \tag{2.48}$$

is conserved, where the integral is taken between the bounce points (Northrop & Teller 1960). The rapid bouncing enforces parity symmetry along the magnetic-field direction. A direct result of both μ and J conservation is then (2.38). The correspondence can be seen more directly by combining (2.27), (2.33), (2.37), and (2.38) to obtain

$$\frac{\tilde{p}_\parallel}{\tilde{p}_{\parallel 0}} \frac{\partial \ell}{\partial \ell_0} = 1, \tag{2.49}$$

which is consistent with the conservation of J as defined in (2.48).

Thus, the conservation of μ and J in magnetised, collisionless plasmas provides a concrete example in which the assumptions made in § 2.2 hold, and (2.41) and (2.42) yield accurate EoSs. However, the general approach we have presented here shows that adiabaticity in the fluid-dynamical context arises due to specific symmetries and phase-space conservation properties of the distribution function. It is best highlighted

Downloaded from https://www.cambridge.org/core. UNIVERSIDAD AUTONOMA METROPOLITANA, on 19 Nov 2026 at 08:19:22, subject to the Cambridge Core terms of use, available at https://www.cambridge.org/core/terms. https://doi.org/10.1017/S0022377826102232

by our isotropic example in § 2.1 that individual particles are not required to possess adiabatic invariants for adiabatic EoSs to hold, although that is the case for rapidly gyrating, trapped particles in magnetised collisionless plasmas. Consequently, the requirement of particle trapping is not necessary for the double-adiabatic equations (2.41) and (2.42) to be valid. The EoSs would hold as long as our assumptions about the symmetries of f and conservation of phase-space volume and area are true. This is why, for example, the CGL equations are found to hold in homogeneous, magnetised, collisionless plasmas, where trapped particles do not exist.

3. Double-adiabatic equations of state for ultra-relativistic plasmas

To make analytical progress in evaluating (2.41) and (2.42), we now consider the ultra-relativistic limit, $\tilde{p}_\perp, \tilde{p}_\parallel \gg mc$. For ease of notation, we drop the tildes above the rest-frame quantities. We employ the coordinate transformation $p_\perp = p\sqrt{1-\xi^2}$ and $p_\parallel = p\xi$, where ξ is the cosine of the pitch angle with respect to the magnetic field. The pressure-evolution equations (2.41) and (2.42) then simplify to

$$P_\perp = 2c\pi B'^2 \int_0^1 \mathrm{d}\xi \int_0^\infty \mathrm{d}p \, \frac{(1-\xi^2)\; p^3 f_0(p,\xi)}{[\xi^2 + (1-\xi^2)B'^3/n'^2]^{1/2}}, \tag{3.1}$$

$$P_\parallel = 4c\pi \frac{n'^2}{B'} \int_0^1 \mathrm{d}\xi \int_0^\infty \mathrm{d}p \, \frac{\xi^2\; p^3 f_0(p,\xi)}{[\xi^2 + (1-\xi^2)B'^3/n'^2]^{1/2}}. \tag{3.2}$$

The 'total' pressure (2.21), here equal to $(2P_\perp + P_\parallel)/3$, is given by

$$P = \frac{2c\pi}{3}\frac{n'^2}{B'} \int_{-1}^1 \mathrm{d}\xi \int_0^\infty \mathrm{d}p \times p^3[\xi^2 + (1-\xi^2)B'^3/n'^2]^{1/2} f_0(p,\xi), \tag{3.3}$$

and has the value

$$P_0 = \frac{2\pi c}{3} \int_{-1}^1 \mathrm{d}\xi \int_0^\infty \mathrm{d}p \; p^3 f_0(p,\xi) \tag{3.4}$$

at $n' = B' = 1$.

If the initial distribution function is isotropic, i.e. $f_0(p,\xi) = f_0(p)$, the integrals over the momentum magnitude can be replaced by (3.4). In this limit, the expressions for $P_\perp$ and $P_\parallel$ are

$$P'_\perp = B'^2 \, I_\perp\left(\frac{B'^3}{n'^2}\right), \tag{3.5}$$

$$P'_\parallel = \frac{n'^2}{B'} \, I_\parallel\left(\frac{B'^3}{n'^2}\right), \tag{3.6}$$

where

$$I_\perp(A) = -\frac{3}{4}\left[\frac{1}{1-A} + \frac{(A-2)}{(1-A)^{3/2}} \; \mathrm{arsinh}\left(\sqrt{\frac{1}{A}-1}\right)\right], \tag{3.7}$$

$$I_\parallel(A) = \frac{3}{2}\left[\frac{1}{1-A} - \frac{A}{(1-A)^{3/2}} \; \mathrm{arsinh}\left(\sqrt{\frac{1}{A}-1}\right)\right], \tag{3.8}$$

Downloaded from https://www.cambridge.org/core. UNIVERSIDAD AUTONOMA METROPOLITANA, on 19 Nov 2026 at 08:19:22, subject to the Cambridge Core terms of use, available at https://www.cambridge.org/core/terms. https://doi.org/10.1017/S0022377826102232

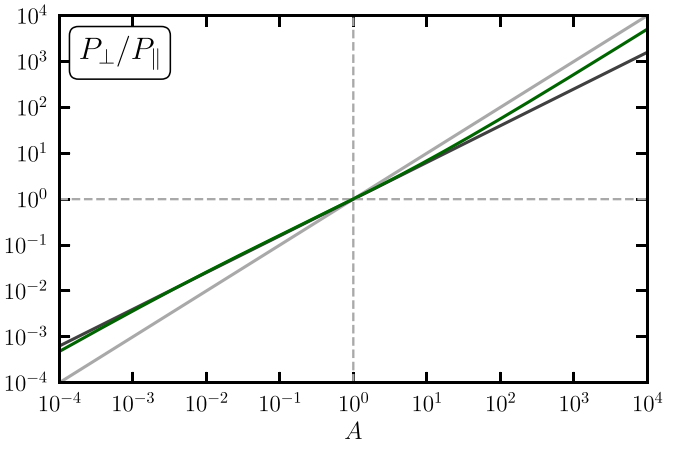


FIGURE 1. Ratio $P_\perp/P_\parallel$ as a function of $A \equiv B'^3/n'^2$ (see (3.10)), shown by the green line. The solid light- and dark-grey lines indicate $P_\perp/P_\parallel = A$ and $P_\perp/P_\parallel = A^{4/5}$, respectively. In the limits $P_\perp/P_\parallel \ll 1$ and $P_\perp/P_\parallel \gg 1$, the ratio scales as $P_\perp/P_\parallel \sim A$, whereas close to isotropy it scales as $P_\perp/P_\parallel \sim A^{4/5}$.

and

$$A \equiv \frac{B'^3}{n'^2}. \tag{3.9}$$

Here, we have also defined $P'_\perp \equiv P_\perp/P_0$ and $P'_\parallel \equiv P_\parallel/P_0$. In the case $A > 1$, the identity $\operatorname{arsinh}\xi = -i\arcsin(i\xi)$ can be used to rewrite (3.7) and (3.8) in an explicitly real form. Key dimensionless physical parameters, *viz.* $\beta_\perp \equiv 8\pi P_\perp/B^2$, $\beta_\parallel \equiv 8\pi P_\parallel/B^2$, and the pressure anisotropy $P_\perp/P_\parallel$, depend only on the parameter A. For example, the latter is

$$\frac{P_\perp}{P_\parallel} = A\frac{I_\perp(A)}{I_\parallel(A)}, \tag{3.10}$$

which we plot in figure 1.

The relations (3.5) and (3.6) are the double-adiabatic EoSs for an ultra-relativistic collisionless magnetised plasma with an initially isotropic distribution function. As the point $t = 0$ is arbitrary, the above EoS holds as long as f is isotropic at some point in time. An appealing property of these relations is their independence of the specific form of $f_0(p)$, provided that most particles contributing to the pressure tensor are ultra-relativistic. If we impose isotropic evolution, $P_\perp = P_\parallel \equiv P$, then setting (3.1) and (3.2) equal to each other yields $B'^3 = n'^2$. Inserting this back into either of the pressure equations gives the expected result for an isotropic ultra-relativistic plasma

$$P'_\perp = P'_\parallel = P' = n'^{4/3}. \tag{3.11}$$

It is useful to consider the EoSs (3.5) and (3.6) in three key asymptotic limits:

(i) large perpendicular pressure, $P_\perp \gg P_\parallel \implies A \gg 1$:

$$P'_\perp = \frac{3\pi}{8}n' B'^{1/2}, \quad P'_\parallel = \frac{3\pi}{4}\frac{n'^3}{B'^{5/2}}; \tag{3.12}$$

Downloaded from https://www.cambridge.org/core. UNIVERSIDAD AUTONOMA METROPOLITANA, on 19 Nov 2026 at 08:19:22, subject to the Cambridge Core terms of use, available at https://www.cambridge.org/core/terms. https://doi.org/10.1017/S0022377826102232

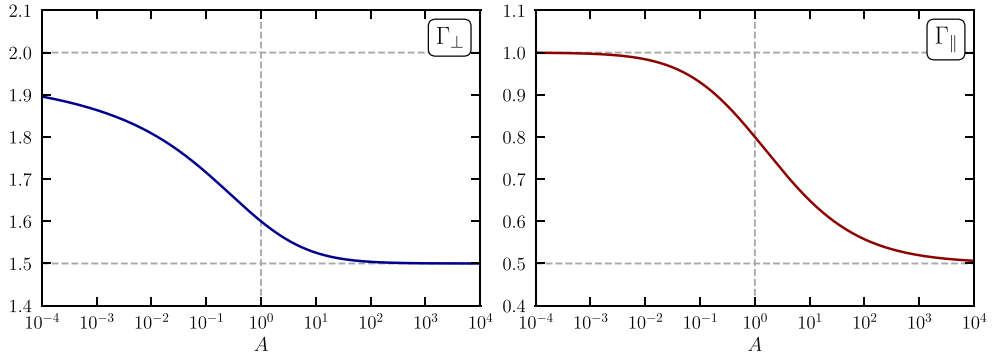


FIGURE 2. Generalised adiabatic indices $\Gamma_\perp$ (left) and $\Gamma_\parallel$ (right), defined in § 3.1, as functions of the pressure anisotropy parameter $A = B'^3/n'^2$. The pressure-evolution equations written in terms of these generalised adiabatic indices are (3.15). The dashed vertical lines correspond to the point $A = 1$, i.e. isotropic plasma.

(ii) almost isotropic plasma, $P_\perp \approx P_\parallel \implies |A-1| \ll 1$:

$$P'_\perp = (n'B')^{4/5}, \quad P'_\parallel = \left(\frac{n'^3}{B'^2}\right)^{4/5}; \tag{3.13}$$

(iii) large parallel pressure, $P_\perp \ll P_\parallel \implies A \ll 1$:

$$P'_\perp = \frac{3}{4}B'^2 \ln\left(\frac{n'^2}{B'^3}\right), \quad P'_\parallel = \frac{3}{2}\frac{n'^2}{B'}. \tag{3.14}$$

The asymptotic limits of significant pressure anisotropy agree with the preliminary, heuristic discussion in Gedalin & Oiberman (1995), except for the logarithmic correction in (3.14), which arises from a careful treatment of the limit $P_\perp \ll P_\parallel$. In such highly anisotropic regimes, the EoSs can be derived straightforwardly from scaling arguments. For example, when $P_\perp \gg P_\parallel$, we have $\gamma \propto p_\perp$. From the conservation of μ (2.47), the perpendicular momentum scales as $p_\perp \propto B^{1/2}$. Conservation of J (2.48) implies $p_\parallel \propto n/B$. Substituting these scalings into (2.40), we find $P_\perp \propto nB^{1/2}$ and $P_\parallel \propto n^3/B^{5/2}$. A similar argument applies in the limit $P_\parallel \gg P_\perp$, where $\gamma \propto p_\parallel$, yielding $P_\perp \propto B^2$ and $P_\parallel \propto n^2/B$. This discussion also implies that the EoSs obtained in the asymptotic limits $P_\perp \gg P_\parallel$ and $P_\parallel \gg P_\perp$ hold even if f_0 is not isotropic, as found in Gedalin & Oiberman (1995), and as can be shown directly from (3.1) and (3.2).

3.1. *Generalised adiabatic indices*

For ease of use in plasma fluid models, we express $I_\perp$ and $I_\parallel$ in the form of power laws, $I_\perp(A) = A^{\Gamma_\perp - 2}$ and $I_\parallel(A) = A^{\Gamma_\parallel - 1}$, where $\Gamma_\perp$ and $\Gamma_\parallel$ are, in general, functions of A. The pressure-evolution equations (3.5) and (3.6) are then

$$P'_\perp = B'^2\left(\frac{n'^2}{B'^3}\right)^{2-\Gamma_\perp}, \quad P'_\parallel = \frac{n'^2}{B'}\left(\frac{n'^2}{B'^3}\right)^{1-\Gamma_\parallel}. \tag{3.15}$$

We refer to $\Gamma_\perp$ and $\Gamma_\parallel$ as the perpendicular and parallel generalised adiabatic indices, respectively, and plot them as a function of A in figure 2. The values of $\Gamma_\perp$ and $\Gamma_\parallel$

Downloaded from https://www.cambridge.org/core. UNIVERSIDAD AUTONOMA METROPOLITANA, on 19 Nov 2026 at 08:19:22, subject to the Cambridge Core terms of use, available at https://www.cambridge.org/core/terms. https://doi.org/10.1017/S0022377826102232

in the asymptotic limits of A can be found by comparing (3.15) with (3.12), (3.13) and (3.14). Close to isotropy, $|A-1| \ll 1$, $(\Gamma_\perp, \Gamma_\parallel) = (8/5, 4/5)$ and for $A \gg 1$, $(\Gamma_\perp, \Gamma_\parallel) = (3/2, 1/2)$. When $A \ll 1$, $\Gamma_\parallel = 1$, but $\Gamma_\perp$ tends to 2 only slowly due to the logarithmic dependence of $I_\perp(A)$ on A in this limit.

3.2. *Eulerian formulation*

We have so far worked in a Lagrangian framework with respect to the bulk velocity $\boldsymbol{u}$. Numerical implementation of (3.1) and (3.2), however, is often simpler when the EoSs are written in their Eulerian form

$$\frac{\mathrm{d}}{\mathrm{d}t}\left(\frac{P_\perp}{B^2 I_\perp(A)}\right) = 0, \quad \frac{\mathrm{d}}{\mathrm{d}t}\left(\frac{P_\parallel B}{n^2 I_\parallel(A)}\right) = 0. \tag{3.16}$$

Here, $\mathrm{d}/\mathrm{d}t \equiv \partial/\partial t + \boldsymbol{u}\cdot\boldsymbol{\nabla}$ is the convective time derivative, and $A = A(P_\perp/P_\parallel)$ is related implicitly to the pressures by (3.10). The absence of primed quantities makes these equations straightforward to implement in fluid simulations and facilitates the inclusion of additional non-ideal effects, such as cooling.

4. PIC simulations of ultra-relativistic plasma in a compressing box

To test the double-adiabatic EoSs that we have derived, we carry out fully kinetic, two-dimensional PIC simulations using the relativistic code `OSIRIS` (Fonseca *et al.* 2002). We employ a set-up in which an electron–positron plasma is compressed perpendicularly to a straight uniform magnetic field of initial strength B_0. As a result, both the density and magnetic field increase while maintaining $B' = n'$, meaning that, in this set-up, $A = n'$. We initialise each species with a Maxwell–Jüttner distribution

$$f(\boldsymbol{p}) \propto e^{-\gamma m_e c^2/T_0}, \tag{4.1}$$

with temperature $T_0 = 10\, m_e c^2$ and density n_0 such that $\beta_0 = 8\pi n_0 T_0/B_0^2 = 1$ for both species. We choose these parameters in order to postpone the onset of pressure-anisotropy-driven kinetic instabilities (Chandrasekhar *et al.* 1958; Hasegawa 1969; Southwood & Kivelson 1993; Bott *et al.* 2024), which will eventually break the double-adiabatic evolution. The full details of our simulations are discussed in Appendix A.

We observe that, as a result of the compression, both the true and modified pressures increase with time as predicted. Plots of these quantities obtained from our simulations, as functions of n', are shown in the left panel of figure 3. We find excellent agreement with our theoretical predictions. The evolution of $P_\perp$ and $P_\parallel$ satisfies (3.5) and (3.6) with $B' = n'$. Figure 3 shows that at values of n' close to unity, i.e. for small anisotropies, $P'_\perp = n'^{8/5}$ and $P'_\parallel = n'^{4/5}$, as expected from (3.13), until $n' \approx 3.2$, when the assumption $P_\perp \sim P_\parallel$ no longer holds and the full pressure equations are required. Our simulations also show that the evolution of $\hat{P}'_\perp$ and $\hat{P}'_\parallel$ is precisely captured by (2.46).

Eventually, when $\Delta \sim 1/\beta_\perp$, around $n' \approx 6.3$, we begin to observe an increase in magnetic energy, indicating the onset of the relativistic mirror instability (Galishnikova, Philippov & Quataert 2023). As a result of the microscale fluctuations in the magnetic field excited by the instability, double-adiabatic evolution breaks down at $n' \approx 7.9$ due to μ no longer being conserved. Hence, the pressures and modified pressures cease to satisfy (3.5), (3.6), and (2.46). In future work, we

Downloaded from https://www.cambridge.org/core. UNIVERSIDAD AUTONOMA METROPOLITANA, on 19 Nov 2026 at 08:19:22, subject to the Cambridge Core terms of use, available at https://www.cambridge.org/core/terms. https://doi.org/10.1017/S0022377826102232

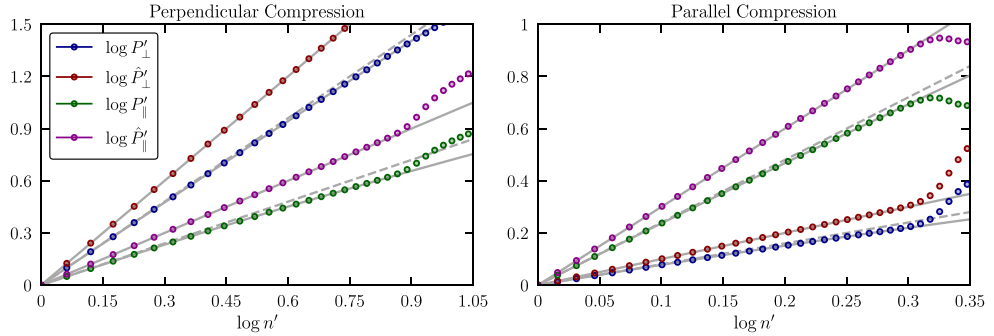


FIGURE 3. The true (2.40) and modified (2.43) pressures, calculated from PIC simulations of plasma undergoing compression perpendicular (left panel) and parallel (right panel) to the magnetic field, plotted as functions of the normalised density n'. In the perpendicular-compression case, $B' = n'$, while in the parallel case $B' = 1$. The theoretical predictions given by (3.5), (3.6), and (2.46) are shown as solid grey lines. In the left panel, the grey dashed lines correspond to $P'_\perp = n'^{8/5}$ and $P'_\parallel = n'^{4/5}$, and in the right panel to $P'_\perp = n'^{4/5}$ and $P'_\parallel = n'^{12/5}$. At larger compressions, a clear departure from double-adiabatic theory is observed due to the excitation of the relevant pressure-anisotropy-driven kinetic instabilities.

will further study the late-time evolution of these systems, where the onset of kinetic instabilities becomes important.

To check the general form of the ultra-relativistic pressure-evolution equations (3.5) and (3.6), we also ran simulations in which the plasma was compressed parallel to the magnetic field. The simulation results are shown in the right panel of figure 3. During such compression, n' still increases with time, but B' remains fixed at unity. We again found good agreement with our double-adiabatic evolution equations, observing initial growth of the pressures given by $P'_\perp = n'^{4/5}$ and $P'_\parallel = n'^{12/5}$, as predicted by (3.13). In this arrangement, $A = 1/n'^2$, and so during the compression a negative pressure anisotropy arises. As a result, we observe the onset of the firehose instability at $\Delta \sim -1/\beta_\parallel$, occurring at $n' \approx 1.9$. Once the firehose fluctuations become sufficiently large, they begin to scatter particles, thereby double-adiabatic evolution no longer holds due to a breaking of μ conservation. This behaviour is evident in figure 3 at $n' \approx 2.1$, where the pressure and modified-pressure evolutions depart from (3.5), (3.6), and (2.46).

5. Discussion

In this paper, we have shown that phase-space symmetries naturally lead to adiabatic evolution equations for the pressure(s). We did so by treating the distribution function as the density of a six-dimensional, incompressible fluid and demonstrating that imposing such symmetries leads to a self-similar evolution of the distribution function. Taking the appropriate moments of the evolved distribution function then yields adiabatic evolution equations whose form, in general, depends on the initial distribution function.

For a distribution function that is isotropic in the peculiar momentum, such as that of a plasma with efficient pitch-angle scattering, we found an adiabatic EoS for the pressure, which reduces to $P \propto n^{5/3}$ and $P \propto n^{4/3}$ in the non-relativistic and ultra-relativistic limits, respectively. We also considered a distribution whose peculiar-momentum dependence is gyrotropic with respect to a vector field,

Downloaded from https://www.cambridge.org/core. UNIVERSIDAD AUTONOMA METROPOLITANA, on 19 Nov 2026 at 08:19:22, subject to the Cambridge Core terms of use, available at https://www.cambridge.org/core/terms. https://doi.org/10.1017/S0022377826102232

$\boldsymbol{B}$ (the magnetic field), frozen into the bulk flow and symmetric under parity along that direction. We found that such a system satisfies double-adiabatic equations. A natural realisation of this scenario is a collisionless, magnetised plasma, in which particles gyrate rapidly around the magnetic field and undergo fast bounce motion in magnetic mirrors. In this case, the double-adiabatic evolution equations govern the parallel and perpendicular pressures, and our symmetry assumptions are consistent with the conservation of the first and second adiabatic invariants, μ and J.

Through developing this symmetry-based formalism, we extended the double-adiabatic evolution equations of a collisionless plasma to the relativistic regime. For an initially isotropic, ultra-relativistically hot plasma, we found $P_\perp \propto B^2 I_\perp$ and $P_\parallel \propto n^2 I_\parallel / B$, where $I_\perp$ and $I_\parallel$ are functions of the compression ratio B'^3/n'^2, or, equivalently, of the pressure anisotropy. We evaluated these functions in three asymptotic limits and derived the corresponding pressure-evolution equations. Close to isotropy, $P_\perp \propto (nB)^{4/5}$ and $P_\parallel \propto (n^3/B^2)^{4/5}$. When $P_\perp \gg P_\parallel$, we obtained $P_\perp \propto nB^{1/2}$ and $P_\parallel \propto n^3/B^{5/2}$. In the opposite limit, $P_\parallel \gg P_\perp$, we found $P_\perp \propto B^2 \ln(n'^2/B'^3)$ and $P_\parallel \propto n^2/B$. We also expressed our EoSs in a form ready to be implemented in numerical fluid simulations. As the 'initial' time is arbitrary, these EoSs hold if the plasma was, at some point in time, isotropic. We tested these pressure-evolution equations numerically using compressing-box PIC simulations and found excellent agreement with the theoretical predictions.

A limitation of the double-adiabatic EoSs presented here is that, for collisionless plasmas, the distribution function is only gyrotropic if the coordinate $\boldsymbol{r}$ refers to the gyrocentre of the particle. In this case, the statement that the averaged particle velocity is equal to the bulk velocity, $\langle \dot{\boldsymbol{r}} \rangle_{t_{\rm fast}} = \boldsymbol{u}$, neglects magnetic drifts and is therefore valid only in the limit of vanishing gyroradius. Additionally, double adiabaticity requires neglect of heat fluxes and collisions. Incorporating such non-ideal and finite-gyroradius effects would therefore require corrections to the pressure-evolution equations derived here.

Our derivation was also restricted to plasmas with a non-relativistic bulk flow. An extension to the fully relativistic regime is possible and yields the same EoSs, with the time coordinate replaced by the proper time of the bulk flow (Wierzchucka *et al.* 2026*b*). In this regime, n and B denote, respectively, the density and magnetic-field strength in the comoving frame. Constructing a covariant Lagrangian description of phase-space evolution is mathematically involved, owing, e.g., to the need for relativistic Clebsch variables. It turns out to be considerably easier to derive these results from the relativistic drift-kinetic equation (Wierzchucka *et al.* 2026*b*).

The physical set-up that we consider here provides a natural starting point for a study of driven kinetic processes, such as the excitation of the firehose and mirror instabilities, in high-energy plasmas. Existing studies suggest that relativistic effects introduce order-unity modifications to the instability thresholds (Galishnikova *et al.* 2023; Zhdankin *et al.* 2023), yet many aspects of their nonlinear evolution and saturation in the relativistic regime remain poorly understood, in particular, how driven relativistic mirror and firehose instabilities evolve in the nonlinear regime. The relativistic EoSs derived in this work already indicate departures from non-relativistic behaviour. For example, the perpendicular-pressure evolution (3.5) implies that, unlike in the non-relativistic regime, $\beta_\perp = 8\pi P_\perp / B^2$ decreases under compression perpendicular to the magnetic field. As a result, significantly larger compressions are required to trigger instabilities associated with positive pressure anisotropy, suggesting that relativistic collisionless plasmas could be more stable to anisotropy-driven instabilities than their non-relativistic counterparts.

Downloaded from https://www.cambridge.org/core. UNIVERSIDAD AUTONOMA METROPOLITANA, on 19 Nov 2026 at 08:19:22, subject to the Cambridge Core terms of use, available at https://www.cambridge.org/core/terms. https://doi.org/10.1017/S0022377826102232

Our theory of double-adiabatic evolution is relevant to other processes occurring in relativistic plasmas, such as the emission of synchrotron radiation. Recent studies have found that synchrotron radiation generates a negative pressure anisotropy in a cooling plasma, exciting the firehose and maser instabilities (Bilbao & Silva 2023; Zhdankin *et al.* 2023; Bilbao *et al.* 2024). When the firehose instability interacts with the synchrotron cooling instability (Simon & Axford 1967), a two-phase medium forms (Wierzchucka *et al.* 2026*a*). One of the phases is high-β, and its dynamics is dominated by the firehose instability, which keeps the pressure anisotropy pinned to the firehose marginality condition. The second phase is low-β, and therefore no firehose fluctuations exist within it. The EoSs found in this work have enabled an effective description of such a medium using a fluid model in which the two phases have different effective adiabatic indices (Wierzchucka *et al.* 2026*a*). The determination of effective adiabatic indices through double-adiabatic EoSs is also important for jump conditions of magnetised, collisionless shocks (Sironi & Spitkovsky 2009; Sironi, Spitkovsky & Arons 2013; Bret & Narayan 2018).

This work may be important for the study of plasmoid dynamics in magnetic reconnection in both astrophysical (Øieroset *et al.* 2001; Retinò *et al.* 2007) and laboratory (Hare *et al.* 2017; Totorica, Abel & Fiuza 2017) settings. Reversing magnetic-field configurations are unstable and collapse to form current sheets (Furth, Killeen & Rosenbluth 1963). At sufficiently high Lundquist number, these sheets fragment into secondary magnetic islands, or plasmoids (Loureiro, Schekochihin & Cowley 2007; Uzdensky, Loureiro & Schekochihin 2010). In the relativistic regime, magnetic reconnection has been observed to generate extended non-thermal distributions and accelerate particles (Sironi & Spitkovsky 2014; Werner *et al.* 2015). Several mechanisms have been proposed to explain this acceleration and the formation of power-law tails, including plasmoid mergers and Fermi-type processes (Drake *et al.* 2006; Li *et al.* 2018). Double-adiabatic models based on the conservation of μ and J have been used to describe Fermi acceleration, although primarily in the non-relativistic regime (Le *et al.* 2009; Montag *et al.* 2017). PIC simulations of relativistic reconnection have also shown that conservation of the first two adiabatic invariants can energise particles within compressing plasmoids during the 'secondary acceleration phase', following initial acceleration in current sheets (Petropoulou & Sironi 2018; Hakobyan *et al.* 2021). The double-adiabatic EoSs derived here offer a useful model for describing particle energisation within plasmoids formed during relativistic reconnection.

To conclude, in this paper, we have used a symmetry-based approach to extend the double-adiabatic equations to the relativistic regime, providing a ready-to-implement fluid description for collisionless, magnetised relativistic plasmas. The generality of the formalism suggests that it may also be applicable to other systems satisfying similar assumptions, such as the presence of a frozen-in vector field.

Note: right before the submission of this manuscript, we became aware of similar results that were obtained concurrently and independently by Ley, Tran & Zweibel (2026) and submitted simultaneously with this paper. There are two key differences between our work and that of Ley *et al.* (2026). First, they focus on deriving the adiabatic evolution of f using the (homogeneous) drift-kinetic equation, as opposed to phase-space symmetries. Secondly, while we show that the relativistic double-adiabatic equations (3.5) and (3.6) hold for any distribution function that was at some point in time isotropic, Ley *et al.* (2026) limit themselves to an initial Maxwell–Jüttner equilibrium. Additionally, also shortly before submission, we learned about an otherwise unpublished PhD thesis by P. Simeon (2014) containing a preliminary

Downloaded from https://www.cambridge.org/core. UNIVERSIDAD AUTONOMA METROPOLITANA, on 19 Nov 2026 at 08:19:22, subject to the Cambridge Core terms of use, available at https://www.cambridge.org/core/terms. https://doi.org/10.1017/S0022377826102232

calculation of adiabatic indices in relativistic, collisionless plasmas. In one chapter, the expressions (2.41) and (2.42) are derived, and the integrals are evaluated in the limit close to the initial state, i.e. $B' \approx 1$ and $n' \approx 1$, yielding the EoSs (3.13).

Acknowledgements

We thank A.F.A. Bott, P.G. Ivanov, E.J. Kolmes, M. Lyutikov and M.L. Nastac for useful discussions. We are especially thankful to F. Bacchini for giving us access to the compressing-box module in the Zeltron code, which inspired us to pursue this project.

Editor Luís O. Silva thanks the referees for their advice in evaluating this article.

Funding

Simulations were performed at Deucalion (Portugal), funded by FCT MAPs 2: Masers in Astrophysical Plasmas I.P. project 2025.00058.CPCA.A3, and at MareNostrum 5 (Spain), funded by EuroHPC-JU extreme scale access project KEEP: Kinetic Electrodynamics in Extreme Plasmas (EHPC-EXT-2025E02-066). A.W. was supported by a Clarendon Scholarship and the Merton College Tira Wannamethee Scholarship. P.J.B. was supported by a Leverhulme–Peierls Fellowship. A.G.R.T. was supported by US DOE grant DE-SC0024562 and NNSA Center of Excellence DE-NA0003869. The work of A.A.S. and P.J.B. was supported in part by the UK STFC grant ST/W000903/1. A.A.S. and A.W. were also supported in part by the Simons Foundation via the Simons Investigator Award to A.A.S. This research was supported in part by grant NSF PHY-2309135 to the Kavli Institute for Theoretical Physics (KITP).

Declaration of interests

The authors report no conflict of interest.

Appendix A. Details of PIC simulations

To investigate numerically the double-adiabatic EoSs of relativistic plasmas, we use `OSIRIS` (Fonseca *et al.* 2002), a fully relativistic, three-dimensional, highly parallelised PIC code. The PIC numerical method works by solving the equations of motion for charged particles subject to the Lorentz force and by calculating the self-consistent fields on a grid. It is commonly used in plasma physics because of its ability to model particle interactions accurately, thereby allowing the capture of effects beyond the fluid approximation.

We initialised our simulations with a magnetic field $\boldsymbol{B}_0 = B_0\hat{\boldsymbol{x}}$ and allowed spatial variations only in the (x, y) plane. This choice reflects the fact that kinetic processes, such as the mirror instability, produce fluctuations with wave vectors both parallel and perpendicular to the magnetic field. Our plasma consisted of electrons and positrons of mass m_e. At the start of the simulation, each species had a Maxwell–Jüttner distribution (4.1) with temperature $T_0 = 10\, m_e c^2$ and an associated (ultra-relativistic) gyration frequency $\Omega_{e0} = eB_0/3\theta_0 m_e c$, where $\theta_0 \equiv T_0/m_e c^2$. All times and distances were normalised to the initial gyration period Ω_{e0}^{-1} and the Larmor radius $\rho_{e0} = c/\Omega_{e0}$, respectively. We set the initial densities of the positrons and electrons to $n_0 = \omega_{pe}^2 m_e/4\pi e^2$, where ω_{pe} is the (non-relativistic) plasma frequency. As we are interested in purely collisionless dynamics undisturbed by instabilities, we used $\beta_0 = 8\pi n_0 T_0/B_0^2 = 1$, corresponding to $B_0 = 4.47\ \omega_{pe} m_e c/e$ and $\omega_{pe}/\Omega_{e0} = 6.7$.

Downloaded from https://www.cambridge.org/core. UNIVERSIDAD AUTONOMA METROPOLITANA, on 19 Nov 2026 at 08:19:22, subject to the Cambridge Core terms of use, available at https://www.cambridge.org/core/terms. https://doi.org/10.1017/S0022377826102232

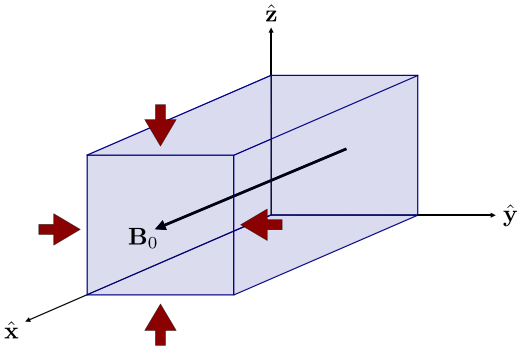


FIGURE 4. Our simulation set-up. The background magnetic field is $\boldsymbol{B}_0 = B_0\hat{\boldsymbol{x}}$, the box is compressed in the z and y directions. Only variations in the (x, y) plane are allowed in the simulation.

Since the EoSs (3.1) and (3.2) express perpendicular and parallel pressures in terms of the density and magnetic-field strength, we set up a large-scale compressing flow in our simulations to introduce controlled variations in B' and n'. The standard PIC treatment of a background, non-relativistic compressing flow, described in Sironi & Narayan (2015), is to solve the PIC equations in a frame comoving with the compressing flow. We implemented this method in `OSIRIS` by modifying the existing shearing-box algorithm (Inchingolo *et al.* 2018). For a general compression, the laboratory coordinate $\boldsymbol{x}$ is related to the comoving coordinate $\boldsymbol{x'}$ by $\boldsymbol{x} = \boldsymbol{L}\boldsymbol{x'}$, where

$$\boldsymbol{L} = \frac{\partial \boldsymbol{x}}{\partial \boldsymbol{x'}} = \begin{pmatrix} q_x & 0 & 0 \\ 0 & q_y & 0 \\ 0 & 0 & q_z \end{pmatrix}, \tag{A1}$$

and q_x, q_y and q_z are time-dependent compression coefficients. To model a compression perpendicular to the magnetic field, we set

$$q_x = 1, \quad q_y = q_z = (1 + St)^{-1}, \tag{A2}$$

where t is time and S is the compression rate. In order for the magnetic field to vary slowly compared with the gyration time, we choose $S/\Omega_{e0} = 10^{-2}$. As a result of this compression, the magnetic field and density satisfy $B' = n' = (1 + St)^2$. Our set-up is summarised in figure 4. We also ran simulations in which the plasma was compressed parallel to the guide field, i.e.

$$q_x = (1 + St)^{-1}, \quad q_y = q_z = 1, \tag{A3}$$

with all other parameters identical to those of the perpendicular-compression simulation. In this case, $n' = 1 + St$, whereas the magnetic field remains constant during the compression.

Our simulations used a spatial resolution $\Delta x = 0.036\,\rho_{e0}$ in each direction and a time step of $\Delta t = 0.0055\,\Omega_{e0}^{-1}$. This ensured that the Courant–Friedrichs–Lewy condition in two dimensions, $c\Delta t/\Delta x < 1/\sqrt{2}$, was satisfied throughout the entire duration of the compression and that Larmor-scale motions were properly resolved.

Downloaded from https://www.cambridge.org/core. UNIVERSIDAD AUTONOMA METROPOLITANA, on 19 Nov 2026 at 08:19:22, subject to the Cambridge Core terms of use, available at https://www.cambridge.org/core/terms. https://doi.org/10.1017/S0022377826102232

The domain size was $L_x \times L_y = 20.1\rho_{e0} \times 20.1\rho_{e0}$, with a corresponding number of cells $N_x \times N_y = 552 \times 552$. We imposed periodic boundary conditions in both directions and used 342 particles per cell with cubic particle shape interpolation.

REFERENCES

BALE, S.D., KASPER, J.C., HOWES, G.G., QUATAERT, E., SALEM, C. & SUNDKVIST, D. 2009 Magnetic fluctuation power near proton temperature anisotropy instability thresholds in the solar wind. *Phys. Rev. Lett.* **103**, 211101.

BEGELMAN, M.C., BLANDFORD, R.D. & REES, M.J. 1984 Theory of extragalactic radio sources. *Rev. Mod. Phys.* **56**, 255.

BESKIN, V.S. & KUZNETSOVA, I.V. 2000 Grad-Shafranov equation with anisotropic pressure. *Astrophys. J.* **541**, 257.

BILBAO, P.J., EWART, R.J., ASSUNÇAO, F., SILVA, T. & SILVA, L.O. 2024 Ring momentum distributions as a general feature of Vlasov dynamics in the synchrotron dominated regime. *Phys. Plasmas* **31**, 052112.

BILBAO, P.J. & SILVA, L.O. 2023 Radiation reaction cooling as a source of anisotropic momentum distributions with inverted populations. *Phys. Rev. Lett.* **130**, 165101.

BLANDFORD, R., MEIER, D. & READHEAD, A. 2019 Relativistic jets from active galactic nuclei. *Annu. Rev. Astron. Astrophys.* **57**, 467.

BOTT, A.F.A., COWLEY, S.C. & SCHEKOCHIHIN, A.A. 2024 Kinetic stability of Chapman–Enskog plasmas. *J. Plasma Phys.* **90**, 975900207.

BOTT, A.F.A., KUNZ, M.W., QUATAERT, E., SQUIRE, J. & ARZAMASSKIY, L. 2025 Thermodynamics and collisionality in firehose-susceptible high-β plasmas. *J. Plasma Phys.* **91**, E136.

BRET, A. & NARAYAN, R. 2018 Density jump as a function of magnetic field strength for parallel collisionless shocks in pair plasmas. *J. Plasma Phys.* **84**, 905840604.

BURCH, J.L., MOORE, T.E., TORBERT, R.B. & GILES, B.L. 2016 Magnetospheric multiscale overview and science objectives. *Space Sci. Rev.* **199**, 5.

CERUTTI, B. & BELOBORODOV, A.M. 2017 Electrodynamics of pulsar magnetospheres. *Space Sci. Rev.* **207**, 111.

CHANDRASEKHAR, S., KAUFMAN, A.N. & WATSON, K.M. 1958 The stability of the pinch. *Proc. R. Soc. Lond. A* **245**, 435.

CHEW, G.F., GOLDBERGER, M.L. & LOW, F.E. 1956 The Boltzmann equation and the one-fluid hydromagnetic equations in the absence of particle collisions. *Proc. R. Soc. Lond. A* **236**, 112.

DRAKE, J.F., SWISDAK, M., CHE, H. & SHAY, M.A. 2006 Electron acceleration from contracting magnetic islands during reconnection. *Nature* **443**, 553.

ECKART, C. 1940 The thermodynamics of irreversible processes. III. Relativistic theory of the simple fluid. *Phys. Rev.* **58**, 919.

FONSECA, R.A. *et al.* 2002 OSIRIS: a three-dimensional, fully relativistic particle in cell code for modeling plasma based accelerators. In *Computational Science — ICCS 2002*, p. 342. Springer.

FURTH, H.P., KILLEEN, J. & ROSENBLUTH, M.N. 1963 Finite-resistivity instabilities of a sheet pinch. *Phys. Fluids* **6**, 459.

GALISHNIKOVA, A., PHILIPPOV, A. & QUATAERT, E. 2023 Polarized anisotropic synchrotron emission and absorption and its application to black hole imaging. *Astrophys. J.* **957**, 103.

GARDNER, C.S. 1959 Adiabatic invariants of periodic classical systems. *Phys. Rev.* **115**, 791.

GEDALIN, M. & OIBERMAN, I. 1995 Generally covariant relativistic anisotropic magnetohydrodynamics. *Phys. Rev. E* **51**, 4901.

HAKOBYAN, H., PETROPOULOU, M., SPITKOVSKY, A. & SIRONI, L. 2021 Secondary energization in compressing plasmoids during magnetic reconnection. *Astrophys. J.* **912**, 48.

HARE, J.D. *et al.* 2017 Anomalous heating and plasmoid formation in a driven magnetic reconnection experiment. *Phys. Rev. Lett.* **118**, 085001.

HASEGAWA, A. 1969 Drift mirror instability in the magnetosphere. *Phys. Fluids* **12**, 2642.

HEGADE, K.R. & STONE, J.M. 2026 Kinetic magnetohydrodynamics and Landau fluid closure in relativity. arXiv: 2604.05058.

Downloaded from https://www.cambridge.org/core. UNIVERSIDAD AUTONOMA METROPOLITANA, on 19 Nov 2026 at 08:19:22, subject to the Cambridge Core terms of use, available at https://www.cambridge.org/core/terms. https://doi.org/10.1017/S0022377826102232

HELLINGER, P. 2007 Comment on the linear mirror instability near the threshold. *Phys. Plasmas* **14**, 082105.

HELLINGER, P., TRÁVNÍČEK, P., KASPER, J.C. & LAZARUS, A.J. 2006 Solar wind proton temperature anisotropy: linear theory and WIND/SWE observations. *Geophys. Res. Lett.* **33**.

HELLINGER, P. & TRÁVNÍČEK, P.M. 2008 Oblique proton fire hose instability in the expanding solar wind: hybrid simulations. *J. Geophys. Res. Space Phys.* **113**.

INCHINGOLO, G., GRISMAYER, T., LOUREIRO, N.F., FONSECA, R.A. & SILVA, L.O. 2018 Fully kinetic large-scale simulations of the collisionless magnetorotational instability. *Astrophys. J.* **859**, 149.

KARGALTSEV, O., CERUTTI, B., LYUBARSKY, Y. & STRIANI, E. 2015 Pulsar-wind nebulae. *Space Sci. Rev.* **191**, 391.

KRUSKAL, M. 1962 Asymptotic theory of Hamiltonian and other systems with all solutions nearly periodic. *J. Math. Phys.* **3**, 806.

KULSRUD, R. 1964 General stability theory in plasma physics. In *Teoria dei plasmi, Rendiconti della scuola internazionale di fisica 'Enrico Fermi', XXV Corso*, p. 54. Academic Press.

KUNZ, M.W., JONES, T.W. & ZHURAVLEVA, I. 2022 Plasma physics of the intracluster medium. In *Handbook of X-Ray and Gamma-Ray Astrophysics*, p. 1. Springer.

KUNZ, M.W., SCHEKOCHIHIN, A.A. & STONE, J.M. 2014 Firehose and mirror instabilities in a collisionless shearing plasma. *Phys. Rev. Lett.* **112**, 205003.

LANDAU, L.D. & LIFSHITZ, E.M. 1987 *Fluid Mechanics* (L.D Landau and E.M. Lifshitz's Course of Theoretical Physics, Volume 6). Pergamon Press.

LE, A., EGEDAL, J., DAUGHTON, W., FOX, W. & KATZ, N. 2009 Equations of state for collisionless guide-field reconnection. *Phys. Rev. Lett.* **102**, 085001.

LEY, F., TRAN, A. & ZWEIBEL, E.G. 2026 On the double-adiabatic equations in the relativistic regime. arXiv: 2603.25594.

LI, X., GUO, F., LI, H. & LI, S. 2018 Large-scale compression acceleration during magnetic reconnection in a low-beta plasma. *Astrophys. J.* **866**, 4.

LOUREIRO, N.F., SCHEKOCHIHIN, A.A. & COWLEY, S.C. 2007 Instability of current sheets and formation of plasmoid chains. *Phys. Plasmas* **14**, 100703.

MELVILLE, S., SCHEKOCHIHIN, A.A. & KUNZ, M.W. 2016 Pressure-anisotropy-driven microturbulence and magnetic-field evolution in shearing, collisionless plasma. *Mon. Not. R. Astron. Soc.* **459**, 2701.

MONTAG, P., EGEDAL, J., LICHKO, E. & WETHERTON, B. 2017 Impact of compressibility and a guide field on Fermi acceleration during magnetic island coalescence. *Phys. Plasmas* **24**, 062906.

NARAYAN, R. & YI, I. 1995 Advection-dominated accretion: underfed black holes and neutron stars. *Astrophys. J.* **452**, 710.

NEWCOMB, W.A. 1961 Lagrangian and Hamiltonian methods in magnetohydrodynamics. *Nucl. Fusion Suppl. Part* **2**, 451.

NORTHROP, T.G. 1963 Adiabatic charged-particle motion. *Rev. Geophys.* **1**, 283.

NORTHROP, T.G. & TELLER, E. 1960 Stability of the adiabatic motion of charged particles in the Earth's field. *Phys. Rev.* **117**, 215.

ØIEROSET, M., PHAN, T.D., FUJIMOTO, M., LIN, R.P. & LEPPING, R.P. 2001 In situ detection of collisionless reconnection in the Earth's magnetotail. *Nature* **412**, 414.

PETROPOULOU, M. & SIRONI, L. 2018 The steady growth of the high-energy spectral cut-off in relativistic magnetic reconnection. *Mon. Not. R. Astron. Soc.* **481**, 5687.

PHILIPPOV, A. & KRAMER, M. 2022 Pulsar magnetospheres and their radiation. *Annu. Rev. Astron. Astrophys.* **60**, 495.

QUATAERT, E. 2003 Radiatively inefficient accretion flow models of Sgr A*. *Astron. Nachr.* **324**, 435.

REES, M.J., BEGELMAN, M.C., BLANDFORD, R.D. & PHINNEY, E.S. 1982 Ion-supported tori and the origin of radio jets. *Nature* **295**, 17.

RETINÒ, A., SUNDKVIST, D., VAIVADS, A., MOZER, F., ANDRÉ, M. & OWEN, C.J. 2007 In situ evidence of magnetic reconnection in turbulent plasma. *Nat. Phys.* **3**, 235.

SCHEKOCHIHIN, A.A. & COWLEY, S.C. 2006 Turbulence, magnetic fields, and plasma physics in clusters of galaxies. *Phys. Plasmas* **13**, 056501.

SCHEKOCHIHIN, A.A., COWLEY, S.C., RINCON, F. & ROSIN, M.S. 2010 Magnetofluid dynamics of magnetized cosmic plasma: firehose and gyrothermal instabilities. *Mon. Not. R. Astron. Soc.* **405**, 291.

Downloaded from https://www.cambridge.org/core. UNIVERSIDAD AUTONOMA METROPOLITANA, on 19 Nov 2026 at 08:19:22, subject to the Cambridge Core terms of use , available at https://www.cambridge.org/core/terms. https://doi.org/10.1017/S0022377826102232

SIMEON, P. 2014 On the acceleration, dynamics, and propagation of cosmic rays. Ph.D. Stanford University.

SIMON, M. & AXFORD, W.I. 1967 Thermal instability resulting from synchrotron radiation. *Astrophys. J.* **150**, 105.

SIRONI, L. & NARAYAN, R. 2015 Electron heating by the ion cyclotron instability in collisionless accretion flows. I. Compression-driven instabilities and the electron heating mechanism. *Astrophys. J.* **800**, 88.

SIRONI, L. & SPITKOVSKY, A. 2009 Particle acceleration in relativistic magnetized collisionless pair shocks: dependence of shock acceleration on magnetic obliquity. *Astrophys. J.* **698**, 1523.

SIRONI, L. & SPITKOVSKY, A. 2014 Relativistic reconnection: an efficient source of non-thermal particles. *Astrophys. J.* **783**, L21.

SIRONI, L., SPITKOVSKY, A. & ARONS, J. 2013 The maximum energy of accelerated particles in relativistic collisionless shocks. *Astrophys. J.* **771**, 54.

SOUTHWOOD, D.J. & KIVELSON, M.G. 1993 Mirror instability: 1. Physical mechanism of linear instability. *J. Geophys. Res. Space Phys.* **98**, 9181.

SYNGE, J.L. 1957 *The Relativistic Gas*. North-Holland Publishing Company and Interscience Publishers.

TOTORICA, S.R., ABEL, T. & FIUZA, F. 2017 Particle acceleration in laser-driven magnetic reconnection. *Phys. Plasmas* **24**, 041408.

UZDENSKY, D.A., LOUREIRO, N.F. & SCHEKOCHIHIN, A.A. 2010 Fast magnetic reconnection in the plasmoid-dominated regime. *Phys. Rev. Lett.* **105**, 235002.

VANDERVOORT, P.O. 1960 The relativistic motion of a charged particle in an inhomogeneous electromagnetic field. *Ann. Phys. (N. Y.)* **10**, 401.

WERNER, G.R., UZDENSKY, D.A., CERUTTI, B., NALEWAJKO, K. & BEGELMAN, M.C. 2015 The extent of power-law energy spectra in collisionless relativistic magnetic reconnection in pair plasmas. *Astrophys. J.* **816**, L8.

WIERZCHUCKA, A., BILBAO, P.J., EWART, R.J., UZDENSKY, D.A. & SCHEKOCHIHIN, A.A. 2026*a* Two-phase structure of synchrotron-cooling-unstable relativistic plasma. arXiv: 2609.07793.

WIERZCHUCKA, A., BILBAO, P.J., UZDENSKY, D.A. & SCHEKOCHIHIN, A.A. 2026*b* Relativistic kinetic magnetohydrodynamics. in preparation.

YOON, P.H., WU, C.S. & DE ASSIS, A.S. 1993 Effect of finite ion gyroradius on the fire-hose instability in a high beta plasma. *Phys. Fluids B* **5**, 1971.

YUAN, F. & NARAYAN, R. 2014 Hot accretion flows around black holes. *Annu. Rev. Astron. Astrophys.* **52**, 529.

ZHDANKIN, V., KUNZ, M.W. & UZDENSKY, D.A. 2023 Synchrotron firehose instability. *Astrophys. J.* **944**, 24.

Downloaded from https://www.cambridge.org/core. UNIVERSIDAD AUTONOMA METROPOLITANA, on 19 Nov 2026 at 08:19:22, subject to the Cambridge Core terms of use, available at https://www.cambridge.org/core/terms. https://doi.org/10.1017/S0022377826102232